Fusion Engineering and Design 134 (2018) 11–21

Contents lists available at ScienceDirect

Fusion Engineering and Design

journal homepage: www.elsevier.com/locate/fusengdes

Cyclic behavior of ceramic pebble beds under mechanical loading

S. Pupeschi[a,*], M. Moscardini[a], Y. Gan[b], R. Knitter[a], M. Kamlah[a]

[a] Institute for Applied Materials, Karlsruhe Institute of Technology (KIT), Germany
[b] School of Civil Engineering, The University of Sydney, Sydney, NSW, 2006, Australia

ARTICLE INFO

Keywords:
Ceramic pebble beds
Wall effects
Discrete element method
Uniaxial compression test
Cyclic loading

ABSTRACT

Uniaxial compression test (UCT) experiments were conducted along with Discrete Element Method (DEM) simulations. The objective was to investigate the effect of the material properties and of the blanket operational parameters (in terms of packing factor, pebble material/size, compressive load and bed height) on the mechanical response of breeder beds subjected to cyclic loading. UCTs were performed with the EU advanced and reference ceramic breeder materials. To investigate the wall effects on the cyclic response of packed beds, a parametric study was performed varying the bed height to pebble size ratio (H/d). To this end monosized commercial zirconia pebbles with different sizes were also used. The numerical experiments were carried out with the KIT-DEM code on pebble assemblies using mixed boundary conditions (periodic and rigid planes). The influence of the bed height, pebble size and pebble material were systematically evaluated to gain an insight about their influence on the macro and micro response of the beds. Thanks to the microscale numerical modelling the macroscale response is presented together with the micro response at the pebble scale. Good agreement was found between experiments and simulations and thus, the KIT-DEM was confirmed to be a reliable predictive tool for the study breeder bed related problems.

1. Introduction and review of the state of the art

Lithium-based ceramics, in the form of packed-pebble beds, were selected as tritium breeder in the solid breeder blanket concepts [1,2]. The qualification of the breeder material for blanket application is required to demonstrate acceptable performances under fusion relevant conditions, this includes the characterization of their thermo-mechanical behavior. A blanket module will experience a cyclic loading due to the burn pulses of the plasma, temperature gradients and a mismatch of the thermal expansion coefficients between the beds and the structural materials results in a cyclic compressive load acting on the breeder beds. Pebble beds show a rather complex thermo-mechanical behavior due to the discrete nature of the individual pebbles. Laboratory investigations along with microscale numerical modelling, e.g. using Discrete Element Method (DEM), can produce full insight into the complex mechanical behavior of the packed beds relating the macroscopic response with the microscopic interactions at the pebble scale.

The Uniaxial Compression Test (UCT, or oedometric compression test) was extensively used to characterize the mechanical response of breeder beds. Several UCT experiments have been carried out by using different facilities and types of pebbles [3–11]. The mechanical behavior of the pebble beds is characterized by nonlinear elasticity accompanied by an irreversible residual strain after the first unloading. This is caused by a significant pebble rearrangement during the first cycle that leads to a densification of the bed. When the bed is subjected to cyclic loading, the largest part of the irreversible residual strain is generated during the first few cycles [11]. Then the compaction of the bed is still progressing, but with smaller increments as the cycling proceeds. This progressive compaction behavior should be quantified in order to effectively control and manage the gap formation that may result in isolated heating zones of breeding zones during operation.

The mechanical behavior of pebble beds can be modelled by either the Discrete Element Method (DEM) or a continuum approach. In the continuum approach a set of phenomenological constitutive equations, based on the effective properties of the beds, are implemented in a Finite Element code to simulate the mechanical behavior of the beds [12]. In the DEM approach, introduced by Cundall and Strack [13], each particle defined by its radius (for spherical particles), mass, physical and mechanical properties, is considered individually. The contact law between particles defines the inter-particle normal and tangential forces. By solving the equations of motion for each single particle composing the assembly and homogenizing the microscopic interactions between the constituent particles, the macroscopic behavior of the granular assembly is derived. DEM has been widely adopted to study the thermomechanical response of breeder pebble bed assemblies. A

* Corresponding author.
E-mail address: simone.pupeschi@kit.edu (S. Pupeschi).

https://doi.org/10.1016/j.fusengdes.2018.06.009
Received 2 October 2017; Received in revised form 31 January 2018; Accepted 11 June 2018

comprehensive survey about the status of ceramic breeder materials thermomechanics R&D can be found [1,14]. The use of DEM for fusion related applications was started by the researchers of University of California Los Angeles (UCLA), who firstly used a DEM approach to study the micromechanics of breeder beds [4,15]. In their following works [16,17], pebbles were packed in cuboidal and cylindrical assemblies confined by elastic walls made of steel and compressed in the axial direction, the stress strain response as well as the internal contact forces were investigated. Assemblies consisting of monosized spherical pebbles (diameter of 1 mm) with an initial packing factor (PF) of 60 ± 0.5% were studied. In their more recent works an open-source DEM code was employed to study the uniaxial compression of monosized packed assemblies with periodic boundary conditions [18] and the thermomechanics of breeder beds experiencing pebble failure [19]. In [18] a modified and randomly distributed young modulus was assigned to the pebbles according to experimental outcomes. An estimation of the percentage of crushed pebbles has also been made.

At Karlsruhe Institute of Technology (KIT) an in-house DEM code was developed by Gan and Kamlah [20]. The original KIT-DEM code was extended by Zhao et al. and Annabattula et al., who implemented the possibility to simulate polydispersed [21] and crushable [22–24] assemblies. Recently the development of the KIT-DEM code has been restarted. The code was further extended to study the bulk behavior of assemblies composed of ellipsoidal particles [25]. The KIT approach [20,21,24,25] was to simulate periodic cubic assemblies of randomly packed pebbles in periodic configuration and under periodic boundary conditions. Doing that, the mechanical response of the bulk of the assembly is represented and wall effects are avoided. The assemblies were generated using a Random Close Packing (RCP) algorithm [26]. The KIT-DEM code was successfully used in previous studies [20,21] to investigate the mechanical behavior of monosized, binary and polydispersed pebble assemblies. The influence of the initial PF [20] and the friction coefficient [21] were investigated as well. Since the previous studies were focused on the first loading/unloading cycle, no repeated cycles were simulated. The characteristic mechanical behavior of granular assemblies subjected to uniaxial compression was accurately reproduced by the DEM simulations. The initial PF as well as the friction coefficient was found to have a profound influence on the mechanical response of the assembly. The monosized assemblies were characterized by a stiffer behavior than binary and polydispersed assemblies. In particular, for an initial PF of approx. 64%, a negligible residual strain was found for monosized assemblies while a residual strain was observed for polydispersed beds.

With application to breeder beds, an ample literature regarding the micromechanics of ceramic beds subjected to a single loading/unloading cycle exist. However, numerical and experimental studies on granular beds undergoing cyclic mechanical loading are comparatively rare. The available experimental and numerical studies [11,16,27] and very recently [28–30] show that cyclic loading leads to a progressive compaction of the bed, resulting in an increase of the effective bed stiffness [16,28,29]. Initially a large volume reduction occurs during the first few cycles, then the compaction saturates as the cycling proceeds. The average and maximum normal contact forces were found to decrease to some extent with cycling, while the coordination number and effective elastic moduli increased [29,30]. In [11], beside the UTC experiments, FEM simulations were carried out as well to study the coupled thermomechanical problem of the HELICA mock-up experiment. A main outcome was that the cyclic thermal stress peaks acting on breeder pebble beds are relaxed, to then saturate after few thermal cycles, due to the pebble bed volume reduction. The DEM numerical studies [16,28] refer to monosized pebble assemblies bounded by elastic walls with an initial packing factor of about 60%. The number of compressive load cycles was limited to few cycles. In the recently published studies [29,30], a commercial DEM code was used to study the cyclic behavior of packed assemblies subjected to uniaxial compression with a considerable number of cycles (about 80). In [29] the influence of sphericity, size distribution and friction coefficient between pebbles on the cyclic behavior of packed beds was assed. The assemblies were uniaxially compressed with both target stress [29,30] and strain [30]. Mixed boundary conditions were used and the initial packing factors varied in the range 60–62%. The simulated pebble size was 1 mm while, when simulated, a very narrow Gaussian size distribution (0.9–1.1 mm) and high sphericity (0.95) were used. The numerical studies [16] [28–30], refer to packing factors actually below the reference value for the solid breeder blanket (BB) concept. Furthermore, in the EU solid BB concept in view of the production process [31], polydispersed beds are used.

This present paper extends an earlier study [32] where DEM simulations were compared with laboratory experiments to gain a preliminary insight on the influence of the cyclic compressive load. In the present study dedicated UCT experiments were performed with both breeder materials and commercial zirconia pebbles to investigate their mechanical response under cyclic loading. To study the wall effect on the cyclic response of packed beds a parametric study was performed varying the bed height to pebble size ratio (H/d). In parallel, numerical simulations were carried out with the KIT-DEM code on pebble assemblies using mixed boundary conditions (periodic and rigid planes). The results of the two approaches, experimental and numerical, were compared. The influence of the bed height, pebble size and pebble material was systematically evaluated to gain insight on the effect of the pebble properties and the blanket operational parameters on the mechanical response of breeder beds subjected to cyclic loading. To provide a representative result for the EU BB, blanket relevant conditions in terms of PF, pebble size, compressive load, bed height and boundary conditions were used. Besides the comparisons between DEM simulations and experiments, rarely reported in literature, this work expands the very limited existing literature about cyclic behavior of breeder beds subjected to mechanical loading.

2. Experiments

The Uniaxial Compression Test (UCT) is one of the few experimental options to get representative parameters of compressed granular materials. Even if differences between the UCT experiment and the real use of the breeder material in the blanket exist, the UCT experiment is one of the very few opportunities to investigate the complex mechanical behavior of granular beds. In UCTs the pebbles, contained in a cylindrical container, are compressed in the axial direction. The bed axially deforms under the applied load while the lateral deformation is inhibited by the container. The stress strain response of the bed is used to characterize its mechanical behavior. Fig. 1 shows a schematic view of the employed oedometer test cell. It consists of a cylindrical measuring cell ①, made of Hastelloy X, of 55 mm inner diameter with a stainless steel disk ② placed in the bottom part. The thickness of the disk can be varied to change the experimental H/D ratio, where H and D are the bed height and diameter, respectively. In the UCT, in order to assure that the mechanical response of the bed is governed by the bulk behavior of the bed, the dimensions of the cylindrical container should be much larger than the diameter of the single pebbles, d. In this study the diameter of the container was kept constant (55 mm) while the bed height was varied to study the influence of the wall effects on the cyclic behavior of ceramic pebble beds. A diameter of 55 mm was considered to be large enough in relation to the maximum diameter of the studied pebbles of 1.2 mm.

Both the EU reference (EU Ref.) and advanced (ACB) tritium breeding materials were investigated. The two materials differ in the chemical composition of the bulk material, the production process and the pebble size distribution. The EU Ref. material consists of about 90 mol% lithium orthosilicate (Li_4SiO_4) and 10 mol% lithium metasilicate (Li_2SiO_3) while the ACB material consist of about 70 mol% Li_4SiO_4 and 30 mol% lithium metatitanate (Li_2TiO_3). The EU Ref. and ACB materials were produced by the melt-spraying process [33] and a melt-based method [34,35], respectively. This results in a difference of the

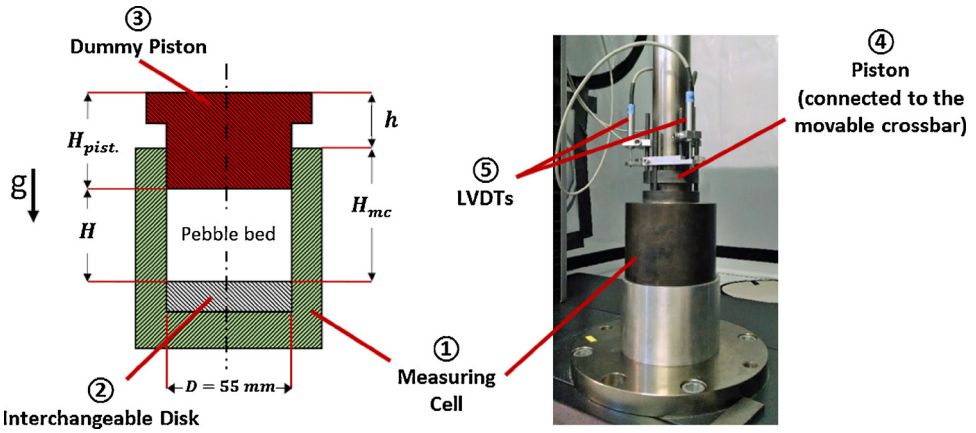

Fig. 1. Schematic view of the odometer test cell and dummy piston for the evaluation of the initial bed height (left), actual photo of the experimental setup (right).

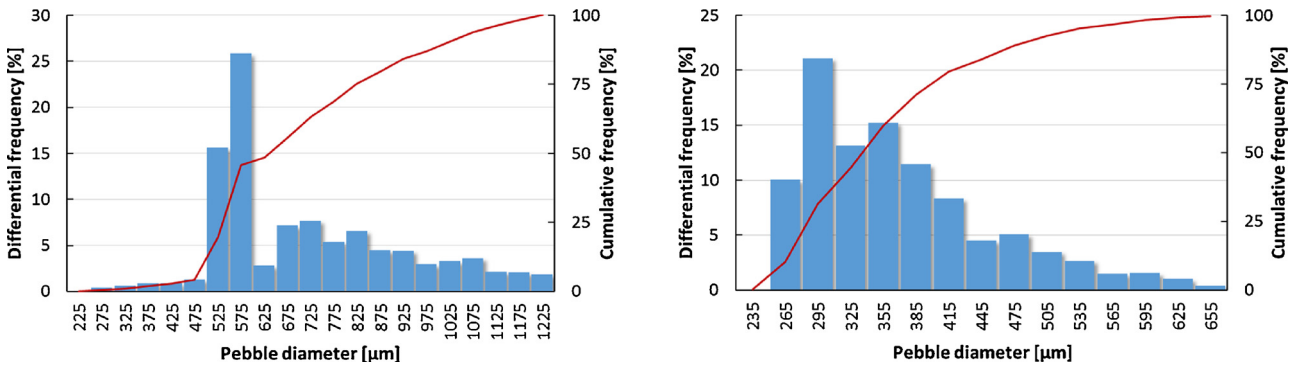

Fig. 2. Size distributions of ACB (left), EU Ref. materials (right).

pebble size distributions as shown in Fig. 2. The EU Ref. material is characterized by a peaked pebble size distribution in the range 0.25-0.65 mm while the ACB material shows a wider size distribution in the range 0.25–1.25 mm. High quality commercial yttria-stabilized zirconia (YTZ) pebbles [36] with different sizes were also employed to investigate the influence of the bed height to pebble size ratio (H/d) on the cyclic response of the packed beds. The zirconia pebbles consist of nearly monosized and perfectly spherical particles, with a sphericity < 1.06 and size variation < 10%. Here, the sphericity of the pebbles was calculated as the ratio of the maximum over the minimum diameter obtained from optical micrographs (2D projection of the pebbles) of a representative sub sample of the selected material. Three diameters were used, namely 1, 0.65 and 0.3 mm.

The selected pebbles were first weighted and then poured into the cylindrical cavity. After filling a dummy piston ③ made of stainless steel was placed above the bed with the only purpose to measure the bed height, see Fig. 1. The initial bed height was measured as $H = H_{mc} + h - H_{pist.}$, where h is the distance between the top of the dummy piston and the top of the measuring cell, while H_{mc} and $H_{pist.}$ are the heights of the measuring cell and of the piston, respectively. The initial PF was calculated according to

$$PF\ [\%] = \frac{m_{pb}}{V_{pb}\,\rho_p} \times 100\,, \tag{2.1}$$

where m_{pb} and V_{pb} are the mass [g] and the volume [cm^3] of the bed, respectively, and ρ_p [g/cm^3] is the bulk density of the pebbles. For the ACB and EU Ref. materials a PF around 64%, consistent with the reference value of the actual EU breeding blanket design, was readily achieved by mechanical vibration. The zirconia pebbles were just poured in the measuring cell and the obtained PF was measured. Other than the ACB and EU Ref. materials, the monosized zirconia pebbles were no further densified to leave a margin to study the densification induced by the cyclic compression. It has to be noted that a BB relevant PF (64%) is difficult to achieve with single size pebbles, since a packing density of 64% represents the random close packing limit for monosized particles [38].

Once the desired PF was achieved, the test cell was placed in the testing machine and the pebble bed was compressed by stainless steel piston ④ connected to the movable crossbar (Fig. 1). The experiments were monitored and controlled by a dedicated LabVIEW program. The beds were cyclically loaded from 20 K Pa up to 6 MPa with a loading speed of 1 MPa/min. The compressive stress of 20 K Pa was applied as preload for the first cycle and kept as minimum stress for the following cycles to guarantee mechanical contact between the piston and the bed. The number of applied compression cycles ranged from 200 to 400 while the investigated initial bed heights were 40, 20 and 10 mm. The maximum compressive load of 6 M Pa was selected because this is considered as the upper limit for the cyclic thermal stress peaks in the breeder zone [37]. Here, the applied macroscopic stress was calculated as the ratio of the applied force, measured by a load cell, to the area of the piston. The bed strain ε [%] was calculated as

$$\varepsilon\ [\%] = \frac{H - d_p}{H} \times 100\,, \tag{2.2}$$

where H is the initial bed height, while d_p is the displacement of the piston measured by means of three Linear Variable Displacement Transducers (LVDTs) ⑤ equally spaced along 360°. Even if the bed deformation [mm] can be measured for experiments at high temperatures, the evaluation of the bed strain ε [%] is only possible at RT when the initial bed height can be accurately measured. At high temperatures ε can only be evaluated assuming the initial bed height, measured at RT, as reference for each temperature. In doing so, the thermal expansion of the experimental setup as well as of the bed are neglected and consequently the calculated ε is not representing the real strain of the bed.

Table 1
Investigated materials and main experimental conditions.

ID	Material	Pebble diameter [mm]	Density [g/cm^3]	PF [%]	H [mm]	H/d [/]
EU Ref.	Li_4SiO_4 + 10 mol% Li_2SiO_3	0.25-0.65	2.30	64 ± 0.1	20; 40	54; 108
ACB	Li_4SiO_4 + 30 mol% Li_2TiO_3	0.25-1.25	2.44	64 ± 0.1	10; 20; 40	14; 28; 56
YTZ - 1	95% ZrO_2 + 5% Y_2O_3	1	6.07	62.65 ± 0.1	10; 20; 40	10; 20; 40
YTZ - 0.65	95% ZrO_2 + 5% Y_2O_3	0.65	6.07	62.7 ± 0.05	20; 40	31; 62
YTZ - 0.3	95% ZrO_2 + 5% Y_2O_3	0.3	6.07	62.7 ± 0.05	20; 40	67; 134

For this reason, the experiments were conducted at room temperature. The physical characteristics and the main experimental conditions of the investigated materials are given in Table 1. For the polydispersed materials the average diameter of the distribution (weighted average on the diameter probability) was used to calculate the H/d ratio.

3. Numerical simulations

Numerical simulations of UCT have been carried out using the KIT-DEM code [20,21,24,25]. The assemblies consisted of perfect spherical particles packed in a virtual box using a Random Close Packing (RCP) algorithm. The assemblies generated by this algorithm accurately reproduce the packing structure obtained in packing experiments [39]. The contacts between pebbles as well as between the pebbles and rigid walls were considered to be purely elastic with normal and tangential interactions. The normal force is evaluated by the Hertzian contact law while the tangential interaction is modelled as a linear elastic force proportional to the tangential displacement unless the Coulomb condition is exceeded. To account for energy dissipation, artificial damping is introduced. The particles' motion, resulting from the calculated contact forces acting on them, is obtained by the numerical integration of the Newton-Euler equations. For a detailed description of KIT-DEM, the reader is referred to [20,21,24,25]. To simulate the UCT experiments, mixed boundary conditions were applied. Rigid planar walls were used to simulate the top and bottom boundaries of the odometer test cell while periodic boundary conditions (PBCs) were applied at the lateral sides of the assemblies. PBCs for the lateral directions allow using a comparably low number of pebbles to achieve the mechanical behavior representative of the assembly where there is no wall effect on the packing structure relevant in the lateral direction, in particular for cyclic loading conditions. While the assembly height was varied to study its influence on the mechanical response, the two lateral dimensions were determined as ten times of the average diameter of the size distribution for polydispersed assemblies or ten times of the particles' diameter for monosized assemblies.

The assemblies were subjected to cyclic loading simulating the uniaxial compression experiments. To this end, the upper wall was moved downwards (or upwards) to cyclically compress (or relax) the bed, while the lower wall was kept fixed as in the experiments. In this way, a strain controlled loading scheme was adopted. A constant strain rate was incrementally applied (or removed) to the assemblies by moving the upper wall at the beginning of each loading step downwards (or upwards). The reaction force acting on the upper wall was then obtained by the calculation of the interaction forces based on the implemented force–displacement law at the pebbles contacts. When the force acting on the upper wall reached the maximum value (σ_{33} = 6 MPa) the bed was unloaded by gradually moving the upper wall upwards until the stress-free configuration, $\sigma_{33} \approx 0$, was reached. Then the assembly was again compressed moving the upper wall downwards in the consequent loading cycle.

Numerical simulations were conducted with both breeder ceramics and commercial zirconia pebbles. The assemblies representing the breeder ceramics were generated with the actual pebble size distributions of the EU Ref. and ACB materials used in the experiments (Fig. 2). To investigate the influence of the sample height four different assemblies were generated with a height of 40, 30, 20 and 10 mm for each breeder material. Regarding the YTZ pebbles five monosized assemblies of a sample height of 20 mm were generated with a pebble size of 2, 1, 0.65, 0.5 and 0.3 mm. This was done to study the influence of the bed height to pebble size ratio (H/d) on the mechanical response of the assemblies. The sample height of 20 mm was selected because it is representative for the breeder zone thickness. While the experiments were performed with 1, 0.65 and 0.3 mm pebbles, in the simulations 0.5 and 2 mm particles were additionally used to broaden the H/d ratio. The material properties of the EU Ref. material used in this study are consistent with those used in earlier studies [20–24]. Due to lack of material properties data, the same mechanical properties were used for the ACB material. The friction coefficient of glass spheres measured in [40] was taken for YTZ pebbles while the mechanical properties of YTZ were taken from [41]. The same friction coefficient was applied for both the inter-particle and particle-wall friction. For each material an assembly with a PF close to the experimental value reported in Table 1 was created. The parameters used to run the simulations are summarized in Table 2.

Table 2
Parameters used in the numerical simulations.

ID	PF [%]	E [GPa]	ν [/]	Inter-particle and particle-wall friction [/]	Pebble size d [mm]	H [mm]	Number of particles	H/d [/]	No. Loading cycles
40-EU Ref.	≈64%	90	0.25	0.1	0.25-0.65	40	5500	56	9
30-EU Ref.						30	4125	42	13
20-EU Ref.						20	2750	28	21
10-EU Ref.						10	1375	14	52
40-ACB	≈64%	90	0.25	0.1	0.25-1.25	40	11400	108	22
30-ACB						30	8550	81	29
20-ACB						20	5700	54	53
10-ACB						10	2850	27	104
YTZ-2	≈62.6%	210	0.25	0.05	2		1195	10	200
YTZ-1					1		2391	20	200
YTZ-0.65					0.65	20	3678	31	100
YTZ-0.5					0.5		4782	40	70
YTZ-0.3					0.3		7970	134	40

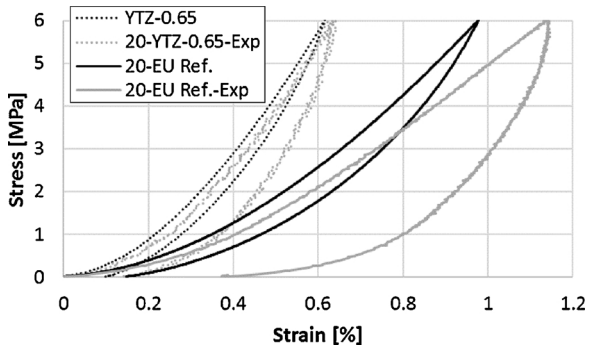

Fig. 3. Comparison between experimental and simulated stress-strain curves for monosized and polydispersed assemblies (1 st loading/unloading cycle).

4. Results and discussion

The macroscale response of the studied assemblies is hereafter presented together with the micro response at the pebble scale. The macroscale response is described by the evolution of macro parameters such as the stress-strain curves and residual strain accumulation. The micromechanical response is studied in terms of axial local packing factor profile, coordination number, contact force distribution and contact force evolution. Since the microscale response of the granular assembly is not experimentally accessible, the micro parameters presented were obtained numerically.

4.1. Macroscale response

Fig. 3 exemplarily shows the experimental and the respective simulated stress-strain curves for monosized and polydispersed assemblies. With a residual strain around 0.1% after the first unloading, the monosized assemblies show a much stiffer response than the polydispersed assemblies of the breeder materials. This reflects both the superior mechanical properties and the size distribution of the YTZ pebbles. In particular, the residual strain is mainly influenced by the size distribution and the friction coefficient between the pebbles, while the slope of the stress strain plot is mainly influenced by the elastic constants of the pebbles.

Comparing the numerical and the experimental results, it can be observed that the DEM simulations captured the different macroscopic behavior between monosized and polydispersed assemblies. For monosized particles both experiments and simulations show a non-linear elastic loading and unloading. Moreover, with a difference of less than 0.1% in term of strain during the unloading, the numerically obtained stress-strain curve shows values very similar to the experimental ones. For polydispersed assemblies both experiments and simulations show a non-linear elastic loading. However, while the simulations show also non-linear elastic unloading, the experiments show a pronounced ‘hook’ shaped non-linear unloading. The difference in the unloading behavior may result from the differences between the simulations and the laboratory experiments and simplifications in the DEM simulations such as the particle shape [25] and smooth surface for the Hertzian contact model [42]. Since the performed DEM simulations were very computationally intensive, in order to reduce the computation time, PBCs were used in lateral direction to minimize the number of pebbles composing the assemblies. However, by using PBCs the effect of the lateral walls on both the mechanical confinement and the near-wall packing structure of the assembly was neglected. Moreover, in the simulation the pebbles were simulated as perfect spherical particles while the real breeder pebbles, even if characterized by a good sphericity, are not perfect spheres. The influence of the aspect ratio on the macroscopic and microscopic response of monosized ellipsoidal particles was addressed in [25], where the shape of the particles was found to noticeably influence the macroscopic mechanical behavior of the assemblies even for deviations of the aspect ratio from 1 by only a few percent. The numerical replication of the laboratory experiment in all its details, even if feasible, would be very computationally intensive because of the very high number of required pebbles. This would have precluded the possibility to simulate multiple loading cycles. Moreover, the aim of the present work was not to quantitatively reproduce the experiment with DEM simulation, but instead to gain an insight into the influences of the pebble properties and the blanket operational parameters on the mechanical response of breeder beds subjected to cyclic loading. To this end, the use of PBCs was unavoidable, while the constraints concerning the use of PBCs were considered to be acceptable. Despite the differences mentioned before the authors are confident that the macro- as well as the micromechanical parameters resulting from the DEM simulations represent a good approximation of the physical reality. Evidence of this is the fact that all the experimentally observed trends were also reproduced by the DEM simulations.

Due to pebble rearrangement and crushing, granular materials show a densification when subjected to cyclic loading that can be accentuated by the magnitude of the alternating loading itself [43]. This is defined as ratcheting of the material which describes the gradual accumulation of permanent deformation. In some cases, the material can adapt to the external excitation and does not accumulate further deformations (shake down condition). Whether the breeder beds will experience a progressive accumulation of plastic deformation, or whether this process will shake down, is essential for the identification of possible gap formation between the breeder bed and the cooling structure. To study the influence of the pebble size on the ratcheting behavior of granular beds, monosized YTZ pebbles were used. Fig. 4 shows the obtained experimental and numerical results in terms of strain accumulation (ε_r) as a function of the number of applied cycles. For all sizes the residual strain is rapidly accumulating during the first cycles. Successively the assemblies begin to accumulate a low but almost constant deformation as the cyclic loading proceeds. The experimental results indicate a lower “long term” strain accumulation for bigger particles although an almost identical strain accumulation rate was observed at the beginning of the cycling for the three investigated particle sizes. The numerical simulations have captured the same behavior as the laboratory

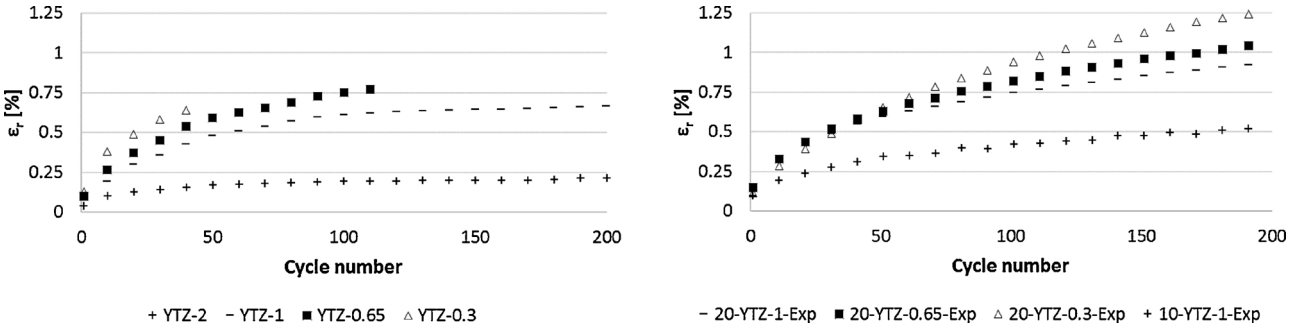

Fig. 4. Numerical (left) and experimental (right) accumulated strain ε_r as a function of the number of cycles for monosized particles.

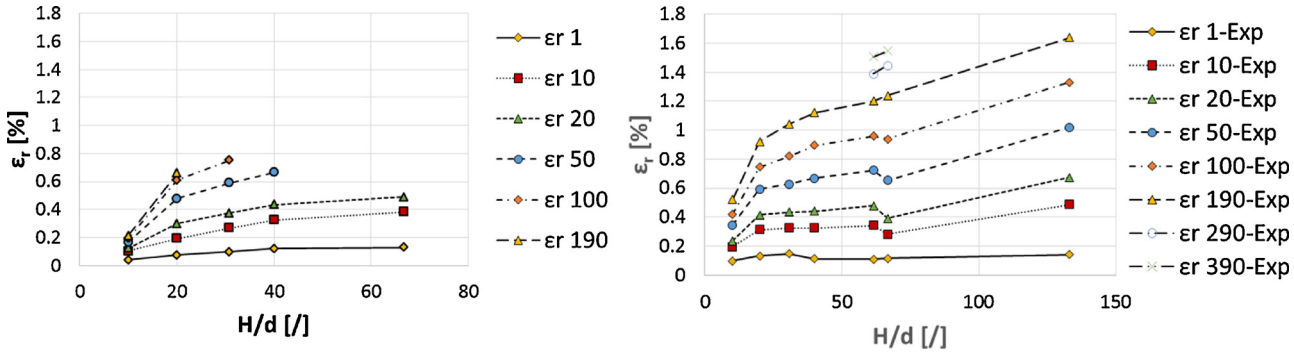

Fig. 5. Accumulated residual strain as a function of the H/d ratio for monosized particles and selected cycles. Numerical (left) and experimental (right) values.

experiments, predicting a lower strain accumulation for bigger particles. Moreover, for the extreme case of YTZ-2 for which the H/d ratio is 10, shake down is reached after 100 cycles. Experiments were also performed with 400 compressive cycles using YTZ-0.65 and YTZ-0.3 pebbles (not shown). Even after 400 cycles the assemblies did not reach shake down.

In Fig. 5 the accumulated residual strain (ε_r) is reported as a function of the H/d ratio at selected compressive cycles. Both, experiments and simulations show an increase of the residual strain with the increase of the H/d ratio. The numerical results show a good agreement with the experimental outcomes. The discontinuity between the experimental values at the two very close H/d ratios (H/d = 62 and 67) is due to the experimental fluctuations.

Fig. 6a shows the experimentally accumulated permanent strain for the breeder materials. Slight differences, in terms of residual strain, were experimentally observed between the investigated bed heights for both materials. The EU Ref. breeder material shows a relatively higher permanent residual strain at higher number of cycles. In particular, the difference in strain between the ACB and the EU Ref. materials after 200 cycles is about 0.5% of strain. For polydispersed assemblies beside the H/d ratio also the shape and the extension of the size distribution play a role in the compaction of the bed [25,32]. For the ACB material the experimental results show a slight decrease of the accumulated permanent residual strain with the reduction of the assembly's height. Fig. 6b and c exemplarily shows the comparison between the numerically and the experimentally accumulated permanent strain for the ACB and EU Ref. materials, respectively. Even if differences in value exist especially for EU Ref. material, the numerical experiments predicted quite accurately the buildup trend of the permanent deformation. As in the experiments, slight differences were numerically observed between the assemblies in the range $20 \leq H \leq 40$ mm (Fig. 6d). However, the numerical results clearly show a significantly lower strain accumulation for the assembly with H = 10 mm.

Experiments and simulations, for both monosized and polydispersed materials, show a continuous increase of the accumulated residual strain which does not saturate with the increase of the H/D ratio, even for H/d values over 100. The increase of the H/d ratio reduces the influence of the walls, for high H/d values the bulk behavior dominates the behavior (later discussed in the paper). The increase of the residual strain with the H/D ratio could be related to the increase of the number of pebbles in the bed's height that ease the pebbles' rearrangement.

4.2. Particle-scale response

The study of the micromechanical parameters can be used to better understand the macro response of the assemblies. The packing structure developed inside the assembly has a substantial influence on the overall micro and macro response of breeder beds. The heat transfer [44] as

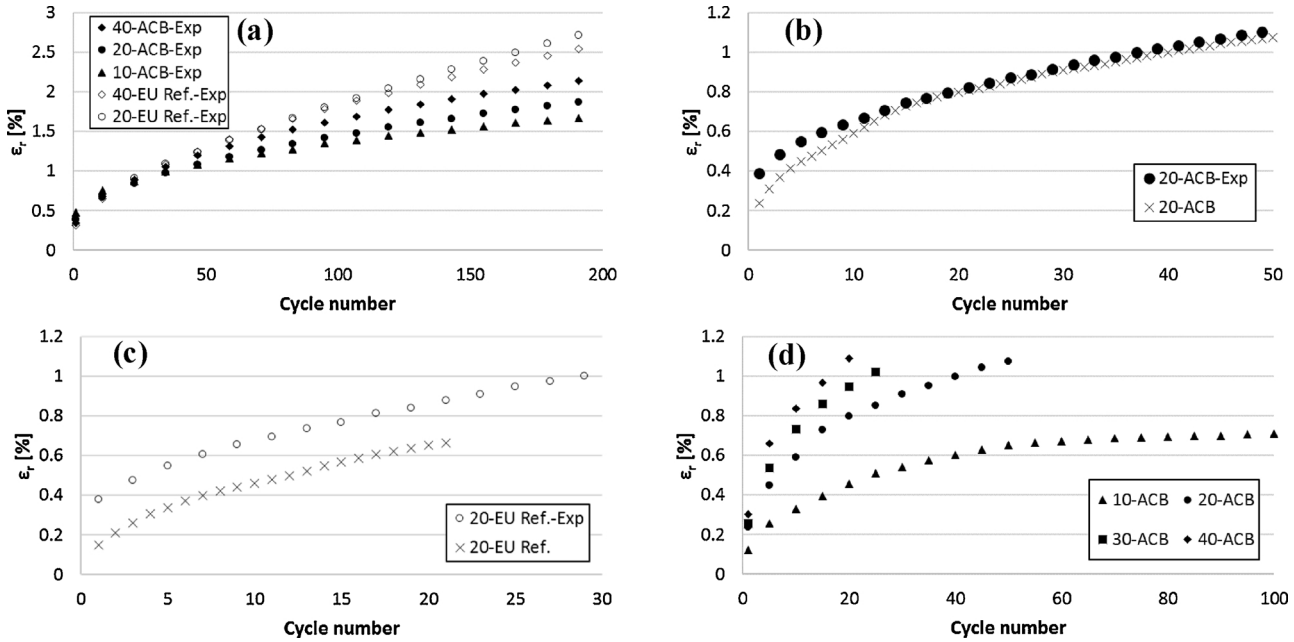

Fig. 6. Accumulated strain ε_r for polydispersed assemblies as a function of the number of cycles (a) experimental, (b) and (c) comparison between experimental and numerical results, (d) numerical results.

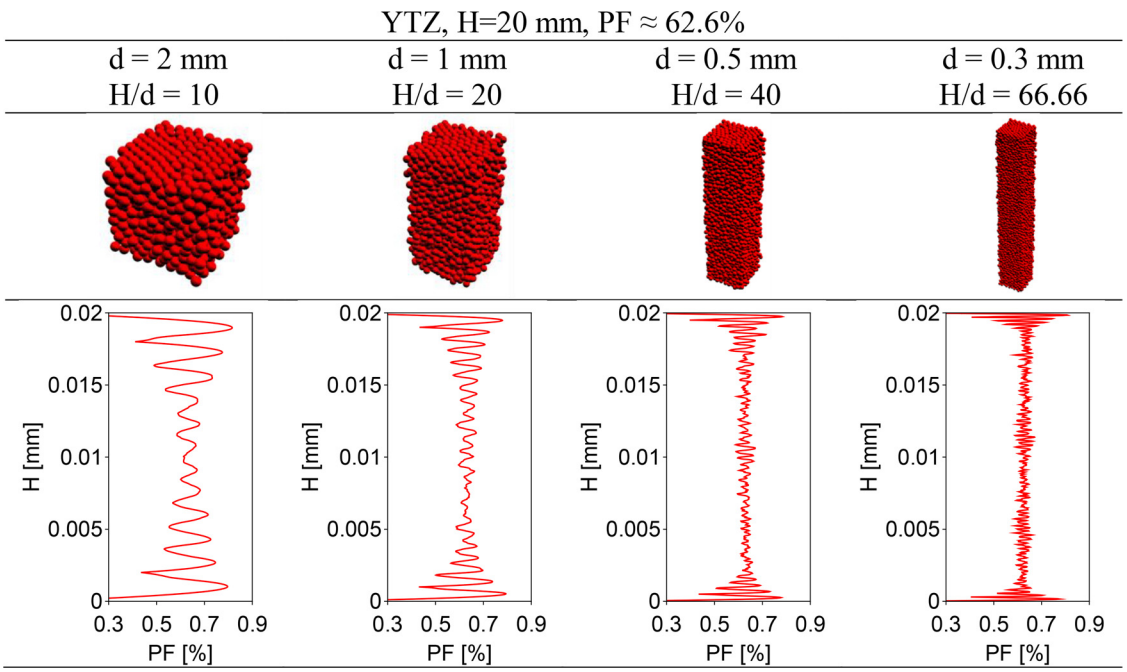

Fig. 7. Calculated axial local packing fraction distribution for monosized assemblies.

well as the mechanical response [9] of the beds are influenced by the packing structure of the particles. Fig. 7 shows the calculated axial local packing factor profile for monosized assemblies. As reported in literature [39,45], and confirmed here, the packing factor shows an oscillatory distribution next to the bounding walls as consequence of the presence of some regularly packed layers of pebbles induced by the walls. The distance of the peak positions of the oscillations correspond to the particle radius. Moving away from the walls, the oscillations are progressively reduced to then vanish at 4–5 times the particle diameter. In this region the regular packing is more and more replaced by the random packing characterizing the bulk zone of the assembly.

In the present study additionally the influence of the H/d ratio on the packing structure was investigated. For low H/d ratios a bulk domain is not developed since the extinction length of the regular packing is comparable with the assembly height. Increasing the H/d ratio (i.e. reducing the pebble diameter), the fraction of the near wall regions is gradually reduced, while the bulk zone dominates the packing structure of the assembly. For the case H/d = 10 no bulk zone was observed, while for H/d = 40 and 66.66 the bulk zone occupies most of the assembly height. The different ratcheting behavior of YTZ-2 in the simulation result in Fig. 4(a), compared with the other pebble sizes, is due to the packing state consisting basically of ordered layers running through bed height. In this assembly the particles have less degree of freedom to move. Thus, even though the micro scale response is not experimentally accessible and a direct comparison with experimental results is not possible, the micromechanical parameters can be used to explain the macroscopic behavior of the assemblies.

Fig. 8 exemplarily shows the axial local packing factor profile for polydispersed assemblies. In the figure the axial distribution of the ACB material is reported. Similar results were obtained for the EU Ref. material.

For polydispersed beds the presence of the walls barely influences the packing structure. The bulk zone dominates the packing structure of the assembly for all investigated assembly heights. Even for the lower investigated height (H = 10 mm) only one fluctuation of the packing factor profile, corresponding to the first layer of pebbles in contact with the boundary walls, can be observed. The observed similar mechanical response between the different bed heights reflects the facts that the bulk zone dominates the packing structure for all investigated assembly heights.

The evolution of the coordination number with cycling for monosized assemblies is reported in Fig. 9. The coordination number (CN) was calculated as $CN = N_c/N_p$, where N_c and N_p are the total number of contacts and the number of particles in the assembly, respectively. The coordination number was evaluated at the maximum load (6 MPa) and at 20 K Pa, representative of the unloaded state. The magnitude of the CN slightly increases with the reduction of the particle size and thus with the increase of H/d. For all investigate sizes the CN increases during the first 10–15 cycles and it tends to saturate afterwards with some fluctuations. The increase of the CN during the initial cycles, with the subsequent stabilization, indicates a compaction of the assembly with a development of a stable network of contacts. Moreover, the evolution of the CN clearly shows that the major pebble rearrangements occur during the initial loading cycles. New contacts are created as a result of compression, resulting in a higher CN at the maximum load. In particular, at 6 MPa the CN is about 10% higher than at the uncompressed state.

Fig. 10 exemplarily shows the evolution of the CN against the cycle number for polydispersed assemblies. In the figure the CN of the ACB material for the four investigated bed heights at 6 MPa and 20 K Pa is reported. Compared with the monosized assemblies, the polydispersed assemblies show a similar evolution of the CN during the cyclic loading even if they show a relatively lower CN value than the monosized assemblies. The CN was found to slightly increase with the reduction of the assembly height.

Fig. 11 shows the Probability Distribution Function (PDF) of the normalized normal forces ($<F_N> = F_N^{ij}/f_{N,ave}$) and normalized maximum normal forces ($<F_{N,max}> = F_{N,max}^{i}/f_{N,ave}$) for YTZ-1 at 6 MPa and 20 K Pa for the first and the last loading cycles. Here F_N^{ij} is the normal force between the contacting particles i and j, $f_{N,ave}$ is the mean normal force inside the assembly and $F_{N,max}^{i}$ is the maximum contact force acting on the particle i. In agreement with the previous studies [16,20], for monosized pebbles the normalized normal force distribution shows a peak at $<F_N> \approx 0.5$ indicating that most particles are subjected to a normal forces lower than $f_{N,ave}$. On the other hand, the peak of maximum normal forces distribution is at $<F_{N,max}> \approx 1.5$ implying that the majority of the particles experience a maximum normal force higher than $f_{N,ave}$. Beside the shape of the distribution, in this study also the

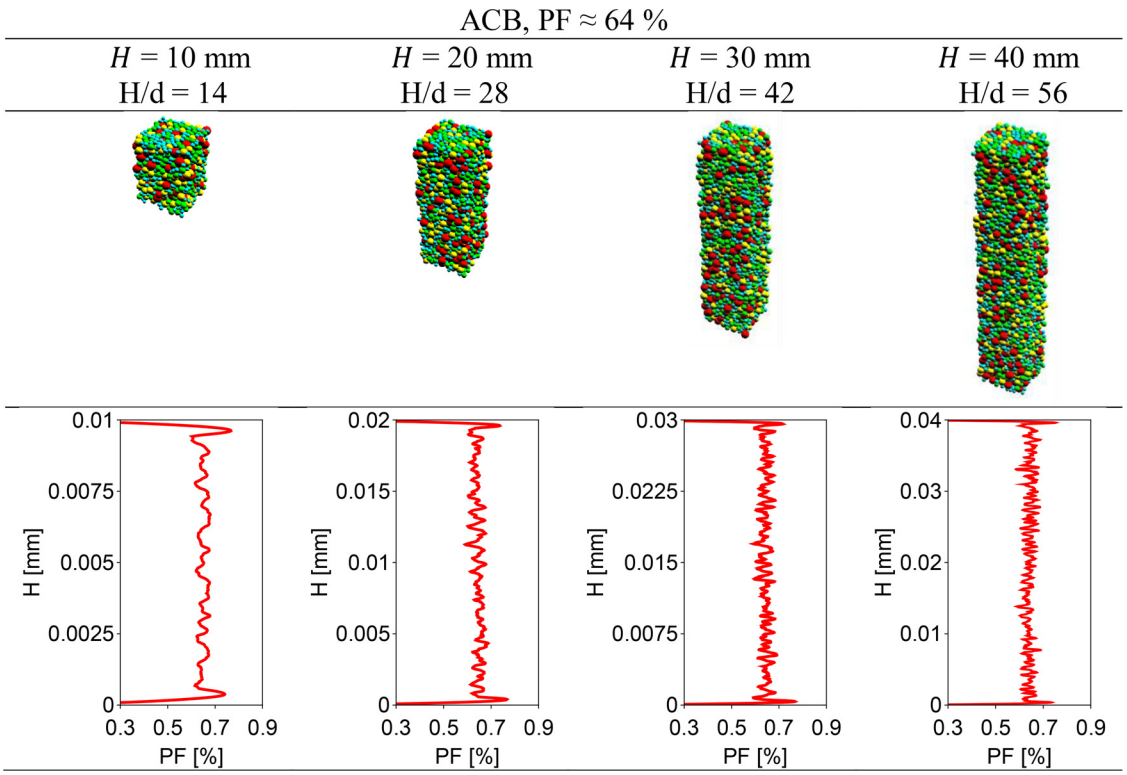

Fig. 8. Calculated axial local packing fraction distribution for polydispersed assemblies (pebbles are colored according to their size.).

influence of the cyclic loading on the PDF was investigated. As shown, both probability distributions are substantially unaffected by the cyclic loading and by the compressive load at which the probability distributions were calculated.

The influence of the pebble size and pebble size distribution on the probability distribution of normalized normal contact forces is exemplary depicted in Fig. 12. Among the monosized assemblies almost identical distributions were obtained for the considered pebble sizes. However, the shape of the PDFs for the polydispersed assemblies differs from those of monosized ones, especially for the normalized maximum normal force distribution. The peak of the $<F_{N,max}>$ distribution is considerably changed. The distribution shows a broader peak slightly shifted to lower values, while the $<F_N>$ distribution shows a similar shape with the peak slightly shifted to lower values. Among the polydispersed assemblies the probability distributions were found to be substantially unaffected by both, the variation of the assembly height and size distribution.

In Fig. 13 the cumulative distribution function (CDF) of the PDF of the normalized normal and maximum normal forces for monosized and polydispersed assemblies are exemplarily shown.

Monosized and polydispersed assemblies show almost the same CDF of the $< F_N >$. It should be noted that about the 40% of the contacts can be classified as "strong" contacts (a contact is defined strong if the normal contact force is greater than the average contact normal force $f_{N,ave}$). The CDF for $<F_{N,max}>$ significantly differs between the monosized and polydispersed assemblies. In particular for the polydispersed assemblies about the 70% of the contacts carry a $f_{N,max}$ greater than $f_{N,ave}$, while for monosized assemblies the contacts experiencing a maximum force greater than the average one rises up to about 80%. However, in polydispersed assemblies about 15% of the contacts experience a maximum force greater than three times $f_{N,ave}$, while this percentage reduces to 6–7% for monosized assemblies. Since the monosized assemblies show almost identical force distributions (Fig. 12) this is valid for all investigated sizes (0.3–2 mm).

Fig. 14 exemplarily shows the evolution of the average and maximum normal contact forces for monosized and polydispersed assemblies at the maximum compressive load. No influence of the bed height was observed for polydispersed beds. In the graphs only the results for 10-ACB and 10-EU Ref. were reported since for these assemblies more cycles were simulated. The magnitude of the contact forces increases with the increase of the particle size. According to their average diameters the $f_{N,ave}$ and $f_{N,max}$ of ACB and EU Ref. polydispersed assemblies lie in between the values of YTZ-1;YTZ-0.65 and YTZ-0.5;YTZ-0.3, respectively. The average diameters of the ACB (0.72 mm) and EU Ref.

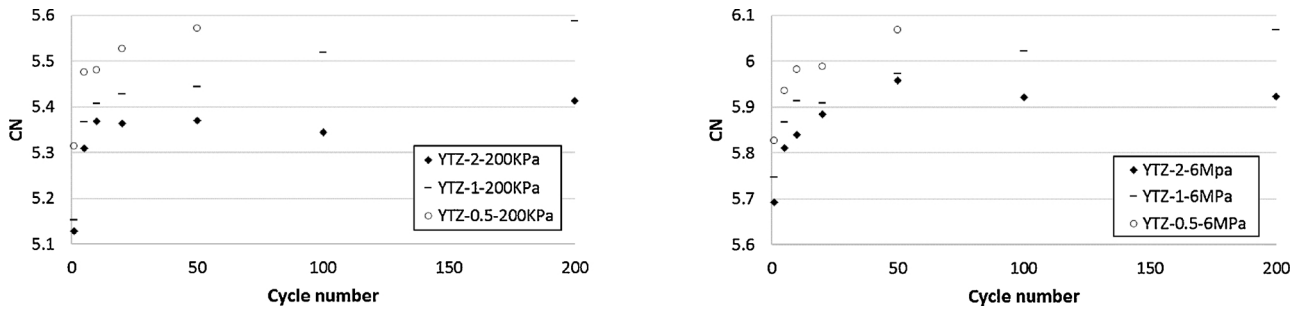

Fig. 9. Evolution of coordination number with cycling for monosized assemblies.

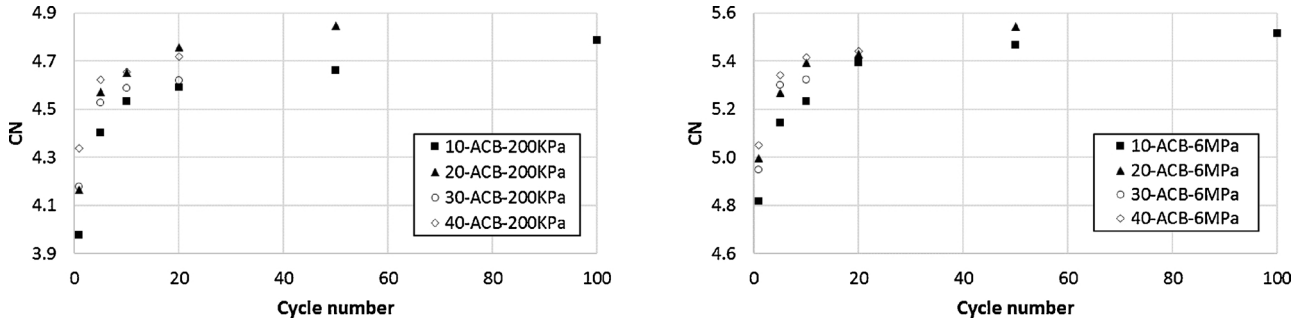

Fig. 10. Evolution of coordination number with cycling for polydispersed assemblies.

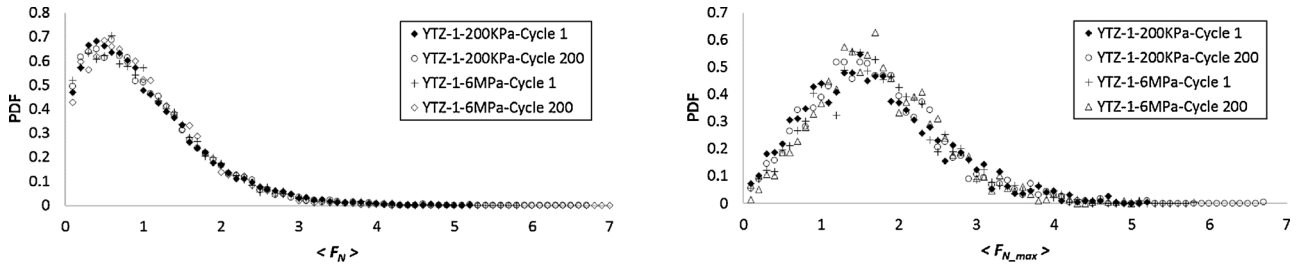

Fig. 11. Influence of cycling loading on the probability density functions of normalized normal forces (left) and normalized maximum normal forces (right) for YTZ-1.

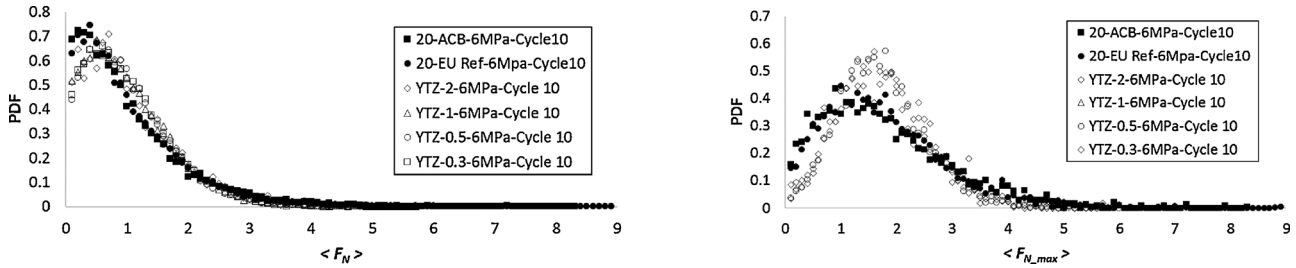

Fig. 12. Influence of size distribution on the probability density functions of normalized normal forces (left) and normalized maximum normal forces (right).

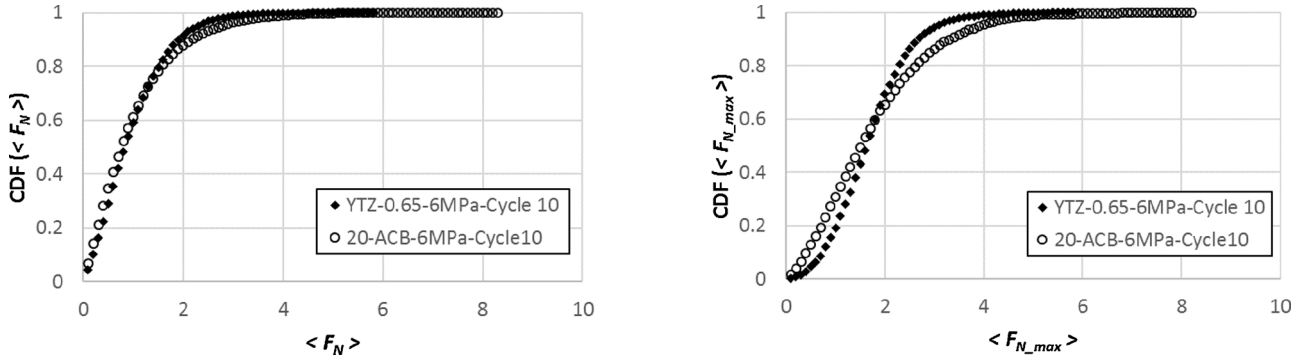

Fig. 13. Influence of size distribution on the cumulative distribution function of normalized normal forces (left) and normalized maximum normal forces (right).

(0.37 mm) materials fit quite well into the respective size ranges of the YTZ. For all pebble sizes and size distributions the average and maximum normal contact forces slightly vary during the first cycles. The average normal contact force that the ceramic breeder material will experience is quite low (about 2.5 N for ACB and 0.65 N for EU Ref.). However, the maximum normal contact force is about 8–9 times the average normal force in the assembly. Very few pebbles will undergo such maximum normal contact force, the majority of the pebbles experience a maximum normal contact force less than 5 times of the average normal force (see Fig. 13). For monosized particles the maximum normal contact force is about 5–6 times the average normal force. However, few monosized pebbles will experience a maximum normal contact force higher than 4 times the average normal force (see Fig. 13).

Fig. 15 illustrates the dependence of the normalized mean and maximum normal forces on the compressive load. The mean and maximum normal forces were normalized with respect to d^2, where d is the pebble diameter for the monosized assemblies and the average diameter of the distribution for polydispersed beds. In the figures the reported values refer to the 20th compressive cycle considering these values as representative for the long term behavior of the bed (see Fig. 14). The d^2-normalized mean and maximum normal forces increase linearly with the compressive load (confirming the results reported in

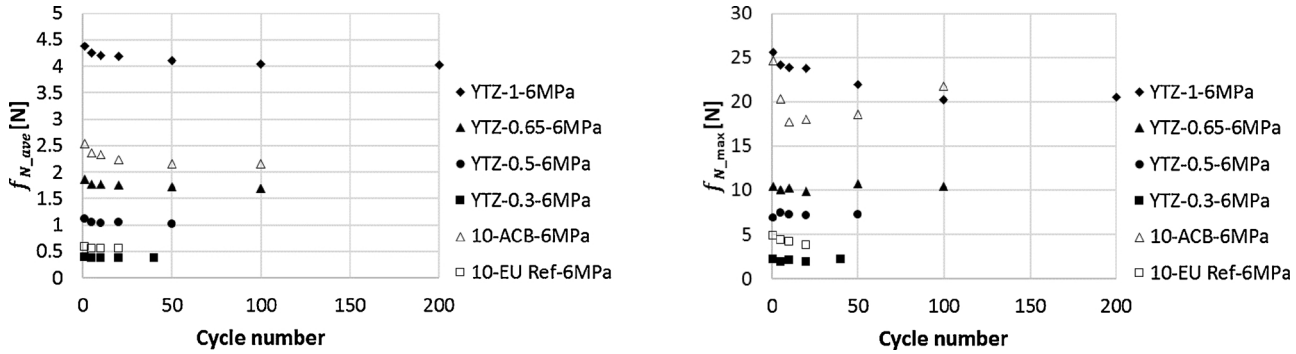

Fig. 14. Evolution of the average (left) and maximum normal contact forces (right).

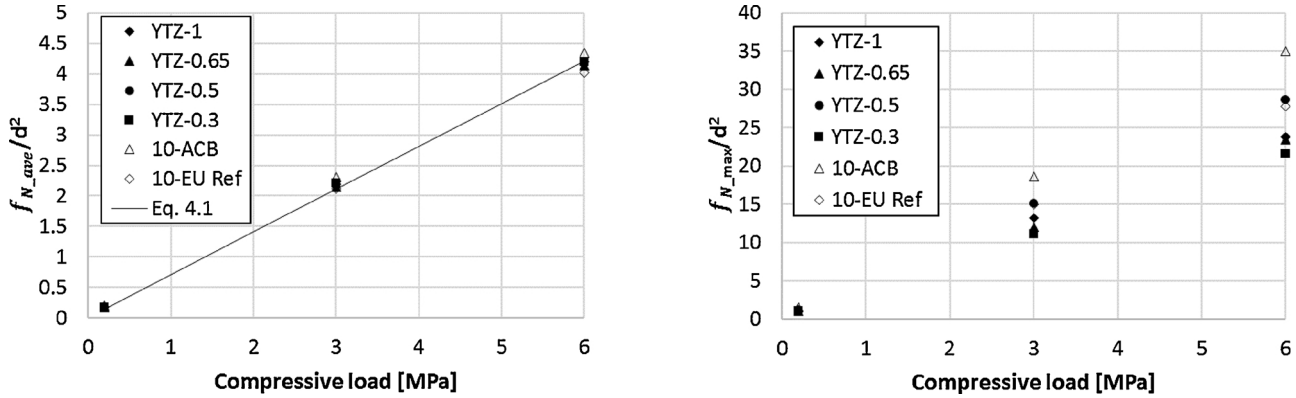

Fig. 15. Mean (left) and maximum (right) normalized normal forces as a function of the compressive load.

[20,21,30],), while the magnitude of the forces themselves strongly reduces with the reduction of the pebble size (see Fig. 14). This reduction was found to be represented by a square dependency on the diameter as can be seen from Fig. 15. The monosized and polydispersed assemblies show a consistent trend of the d^2-normalized mean normal contact forces, while the trends of the d^2-normalized maximum normal forces slightly differ. The investigated assemblies do not show a dependency of the mean and maximum normal forces on the H/d ratio (very similar values were obtained for the investigated heights). The mean normal force can be estimated by

$$f_{N,ave} = 0.702\, d^2\, \sigma \tag{4.1}$$

where σ [MPa] is the uniaxial compressive load and d is the pebble diameter for the monosized assemblies or the average diameter for polydispersed beds. Eq. (4.1) is plotted in Fig. 15 as a continuous line.

As already discussed above, very few pebbles will undergo the maximum normal contact force reported in Figs. 14 and 15. Therefore, based on the study of the CDF of $<F_{N,max}>$ (see Fig. 13), for design purposes and if a very small amount of failing pebbles can be accepted, the maximum normal force acting on the pebbles can be reasonably estimated as

$$f_{N,max} \leq 5 f_{N,ave} \quad polydispersedEU.\ RefandACBpebbles \tag{4.2}$$

$$f_{N,max} \leq 4 f_{N,ave} \quad monosizedpebbles \tag{4.3}$$

5. Conclusions

This work expands the very limited existing literature about the comparisons between DEM simulations and experiments. UCT experiments were conducted along with DEM numerical simulations to investigate the macro- and micromechanical response of breeder beds subjected to cyclic loading. Polydispersed breeder ceramics and monosized commercial zirconia pebbles were used to study the influence of the pebble properties, of the bed height and of the H/d ratio. The KIT-DEM code was confirmed to be a reliable predictive tool for the study of the macro- and microscale response of fusion breeder beds, and trends consistent with experimental outcomes were obtained in terms of stress-strain response and ratcheting behavior.

Monosized assemblies showed a stiffer response and a lower residual strain accumulation than polydispersed assemblies. In this study it was found that for monosized spherical assemblies the experimental and numerical results show a lower strain accumulation for bigger particles and thus an increase of the residual strain with the increase of the H/d ratio. On the other hand, for polydispersed assemblies, the influence of the bed height on their ratcheting behavior was found to be modest.

Results for monosized assemblies show that for low H/d ratios no bulk domain of the packing profile is developed. For polydispersed beds the presence of the walls was found to barely influence the packing structure and the bulk zone dominates the packing structure of the assembly for all investigated assembly heights. This suggests that for the investigated size distributions, even for shallow polydispersed breeder beds (H = 10 mm), the mechanical and thermal behavior of the assembly will by mainly be governed by the bulk behavior. On the contrary, if monosized particles are employed in shallow breeder beds, the particle diameter should be varied accordingly towards a high H/d ratio to assure that the response of the bed is governed by the bulk behavior leading to an isotropic and homogeneous response of the bed.

The evolution of the CN, for both polydispersed and monosized assemblies, clearly shows that the major pebble rearrangements occur during the initial loading cycles. The study of the internal force distribution shows no influence of mechanical cycling, assembly height and size distribution. The shape of the PDFs for the polydispersed assemblies differs from those of monosized ones especially for the normalized maximum normal forces distribution. This results for polydispersed assemblies in a reduction of the number of contacts carrying a maximum normal force greater than the average. On the other hand, to

keep the mechanical equilibrium, in the polydispersed assemblies more contacts will experience a maximum force greater than three times the average than in monosized assemblies. For monosized pebbles, the magnitude of the mean and maximum normal forces reduces with the reduction of the pebble size. The average normal contact force that the ceramic breeder pebbles will experience is quite low (about 2.5 N for ACB and 0.65 N for EU Ref.), while the majority of the pebbles will experience a maximum normal contact force less than 5 times the average normal force. Since the contact forces linearly increase with the compressive load acting on the bed, the reduction of the thermally induced stress peaks with cycling reported in [11] is beneficial for the relaxation of the contact forces, the ratcheting of the bed and the crush probability of the breeder pebbles.

Acknowledgements

Part of this work has been carried out within the framework of the EUROfusion Consortium and has received funding from the Euratom research and training programme 2014-2018 under grant agreement No 633053. The views and opinions expressed herein do not necessarily reflect those of the European Commission.

References

[1] J.G. van der Laan, A.V. Fedorov, S. van Til, J. Reimann, 2016. Ceramic Breeder Materials, Reference Module in Materials Science and Materials Engineering, Current as of 28 October 2015, https://doi.org/10.1016/B978-0-12-803581-8.00733-5.
[2] N. Roux, S. Tanaka, C. Johnson, R. Verrall, Ceramic breeder material development, Fusion Eng. Des. 41 (1998) 31–38.
[3] Alice Y. Ying, Zi Lu, Mohamed A. Abdou, Mechanical behavior and design database of packed beds for blanket designs, Fusion Eng. Des. 39–40 (1998) 759–764.
[4] Z. Lu, A.Y. Ying, M.A. Abdou, Numerical and experimental prediction of the thermomechanical performance of pebble beds for solid breeder blanket, Fusion Eng. Des. 49–50 (2000) 605–611.
[5] J. Reimann, G. Wörner, Thermal creep of Li4SiO4 pebble beds, Fusion Eng. Des. 58-59 (2001) 647–651.
[6] G. Piazza, J. Reimann, E. Günther, R. Knitter, N. Roux, J.D. Lulewicz, Characterisation of ceramic breeder materials for the helium cooled pebble bed blanket, J. Nucl. Mater. 307–311 (2002) 811–816.
[7] J. Reimann, L. Boccaccini, M. Enoeda, A. Ying, Thermomechanics of solid breeder and be pebble bed materials, Fusion Eng. Des. 61–62 (2002) 319–331.
[8] L. Bühler, J. Reimann, Thermal creep of granular breeder materials in fusion blankets, J. Nucl. Mater. 307–311 (2002) 807–810.
[9] J. Reimann, D. Ericher, G. Wörner, Influence of pebble bed dimensions and filling factor on mechanical pebble bed properties, Fusion Eng. Des. 69 (2003) 241–244.
[10] J. Reimann, H. Harsch, Thermal creep of beryllium pebble beds, Fusion Eng. Des. 75–79 (2005) 1043–1047.
[11] C. Zhang, A. Ying, M.A. Abdou, Y. Park, Ceramic breeder pebble bed packing stability under cyclic loads, Fusion Eng. Des. 109–111 (2016) 267–271.
[12] Y. Gan, M. Kamlah, Identification of material parameters of a thermo-mechanical model for pebble beds in fusion blankets, Fusion Eng. Des. 82 (2007) 189–206.
[13] P.A. Cundall, O.D.L. Strack, A discrete numerical model for granular assemblies, Geotechnique 29 (1) (1979) 47–65.
[14] A. Ying, J. Reimann, L. Boccaccini, M. Enoeda, M. Kamlah, R. Knitter, Y. Gan, J.G. van der Laan, L. Magielsen, P.A. Di Maio, G. Dell'Orco, R.K. Annabattula, J.T. Van Lew, H. Tanigawa, S. van Til, Status of ceramic breeder pebble bed thermomechanics R&D and impact on breeder material mechanical strength, Fusion Eng. Des. 87 (2012) 1130–1137.
[15] A.Y. Ying, H. Huang, M.A. Abdou, Numerical simulation of ceramic breeder pebble bed thermal creep behavior, J. Nucl. Mater. 307–311 (2002) 827–831.
[16] Z. An, A. Ying, M. Abdou, Application of discrete element method to study mechanical behaviors of ceramic breeder pebble beds, Fusion Eng. Des. 82 (2007) 2233–2238.
[17] Z. An, A. Ying, M. Abdou, Numerical characterization of thermo-mechanical performance of breeder pebble beds, J. Nucl. Mater. 367–370 (2007) 1393–1397.
[18] J.T. Van Lew, Y. Park, A. Ying, M. Abdou, Modifying Young's modulus in DEM simulations based on distributions of experimental measurements, Fusion Eng. Des. 98–99 (2015) 1893–1897.
[19] J.T. Van Lew, A. Ying, M. Abdou, A discrete element method study on the evolution of thermomechanics of a pebble bed experiencing pebble failure, Fusion Eng. Des. 89 (2014) 1151–1157.
[20] Y. Gan, M. Kamlah, Discrete element modelling of pebble beds: with application to uniaxial compression tests of ceramic breeder pebble beds, J. Mech. Phys. Solids 58 (2010) 129–144.
[21] R.K. Annabattula, Y. Gan, M. Kamlah, Mechanics of binary and polydispersed spherical pebble assembly, Fusion Eng. Des. 87 (2012) 853–858.
[22] S. Zhao, Y. Gan, M. Kamlah, T. Kennerknecht, R. Rolli, Influence of plate material on the contact strength of Li_4SiO_4 pebbles in crush tests and evaluation of the contact strength in pebble–pebble contact, Eng. Fract. Mech. 100 (2013) 28–37.
[23] S. Zhao, Y. Gan, M. Kamlah, Failure initiation and propagation of Li_4SiO_4 pebbles in fusion blankets, Fusion Eng. Des. 88 (2013) 8–16.
[24] R.K. Annabattula, Y. Gan, S. Zhao, M. Kamlah, Mechanics of a crushable pebble assembly using discrete element method, J. Nucl. Mater. 430 (2012) 90–95.
[25] M. Moscardini, Y. Gan, R.K. Annabattula, M. Kamlah, A discrete element method to simulate the mechanical behavior of ellipsoidal particles for a fusion breeding blanket, Fusion Eng. Des. 121 (2017) 22–31.
[26] W.S. Jodrey, E.M. Tory, Computer simulation of close random packing of equal spheres, Phys. Rev. A 32 (4) (1985) 2347–2351.
[27] H. Tanigawa, Y. Tanaka, M. Enoeda, Packing behaviour of a Li_2TiO_3 pebble bed under cyclic loads, J. Nucl. Mater. 417 (1-7) (2011) 703–705.
[28] X. Wang, M. Ye, H. Chen, Computational study on the behaviors of granular materials under mechanical cycling, J. Appl. Phys. 118 (2015) 174901.
[29] H. Zhang, H. Guo, M. Ye, Z. Li, H. Huang, Investigation on the packing behaviors and mechanics of Li4SiO4 pebble beds by discrete element method, Fusion Eng. Des. (2017), http://dx.doi.org/10.1016/j.fusengdes.2017.04.049.
[30] H. Zhang, H. Guo, T. Shi, M. Ye, H. Huang, Z. Li, Cyclic loading tests on ceramic breeder pebble bed by discrete element modeling, Fusion Eng. Des. 118 (2017) 40–44.
[31] W. Pannhorst et al., "Production Process of Lithium Orthosilicate Pebbles", Fusion Tech. 1998, Proceedings of 20th Symposium on Fusion Technology, Sept. 7-11, 1998, Marseille, France, B. Beaumont, P. Libeyre, B. de Gentile, G. Tonon (Eds.), Vol. 2, 1441-1444.
[32] S. Pupeschi, R. Knitter, M. Kamlah, Y. Gan, Numerical and experimental characterization of ceramic pebble beds under cycling mechanical loading, Fusion Eng. Des. 112 (2016) 162–168.
[33] W. Pannhorst, V. Geiler, G. Räke, B. Speit, D. Sprenger, "Production Process of Lithium Orthosilicate Pebbles", Fusion Technol. 1998, Proceedings of 20th Symposium on Fusion Technology, Sept. 7–11, 1998, in: Marseille, France, B. Beaumont, P., Libeyre, B. de Gentile, G. Tonon (Eds.), Vol. 2, 1441–1444.
[34] M. Kolb, R. Knitter, U. Kaufmann, D. Mundt, Enhanced fabrication process for lithium orthosilicate pebbles as breeding material, Fusion Eng. Des. 86 (2011) 2148–2151.
[35] R. Knitter, M.H.H. Kolb, U. Kaufmann, A.A. Goraieb, Fabrication of modified lithium orthosilicate pebbles by additions of titania, J. Nucl. Mater. 442 (2013) 433–436.
[36] http://www.tosoh.com/.
[37] Y. Gan, F. Hernandez, D. Hanaor, R. Annabattula, M. Kamlah, P. Pereslavtsev, Thermal discrete element analysis of EU solid breeder blanket subjected to neutron irradiation, Fusion Sci. Technol. 66 (1) (2018) 83–90, http://dx.doi.org/10.13182/FST13-727.
[38] T. Aste, Variations around disordered close packing, J. Phys. 17 (2005) S2361–S2390.
[39] Y. Gan, M. Kamlah, J. Reimann, Computer simulation of packing structure in pebble beds, Fusion Eng. Des. 85 (2010) 1782–1787.
[40] A. Lorenz, C. Tuozzolo, M.Y. Louge, Measurements of impact properties of small, nearly spherical particles, Exp. Mech. 37 (3) (1997) 292–298.
[41] http://www.tosoh.com/our-products/advanced-materials/zirconia-grinding-dispersion-media.
[42] C. Zhai, Y. Gan, D. Hanaor, G. Proust, D. Retraint, The role of surface structure in Normal contact stiffness, Exp. Mech. 56 (2016) 359–368.
[43] C.T. David, R. García-Rojo, H.J. Herrmann, S. Luding, Hysteresis and creep in powders and grains, Proceeding of the 5th International Conference on Micromechanics of Granular media, Stuttgart, Germany, 18-22 July, 2005.
[44] Y.X. Gan, M. Kamlah, Thermo-mechanical modelling of pebble bed–wall interfaces, Fusion Eng. Des. 85 (2010) 24–32.
[45] J. Reimann, R.A. Pieritz, C. Ferrero, M. Di Michiel, R. Rolli, X-ray tomography investigations on pebble bed structures, Fusion Eng. Des. 83 (2008) 1326–1330.